LETTER

ACS chemical biology

Exploring Drug Target Flexibility Using *in Situ* Click Chemistry: Application to a Mycobacterial Transcriptional Regulator

Nicolas Willand[†,‡,§,∥,*], Matthieu Desroses[†,‡,§,∥], Patrick Toto[†,‡,§,∥], Bertrand Dirié[†,‡,§,∥], Zoé Lens[†,▽,#], Vincent Villeret[†,#], Prakash Rucktooa[†,#], Camille Locht[†,⊥,§], Alain Baulard[†,⊥,§,∥,¶], and Benoit Deprez[†,‡,§,∥,¶,*]

[†]Univ Lille Nord de France, F-59000 Lille, France, [‡]Biostructures and Drug Discovery, INSERM U761, F-59000 Lille, France and UDSL, F-59000 Lille, France, [§]IPL, F-59000 Lille, France, [∥]PRIM, F-59000 Lille, France, [⊥]INSERM U1019, F-59000 Lille, France and CNRS UMR8204, F-59021 Lille, France and Center for Infection and Immunity, F-59019 Lille, France, [#]IRI, USR 3078 CNRS, F-59658 Villeneuve d'Ascq, France, and [▽]Laboratory of Molecular Virology, IBBM, ULB, 6041 Gosselies, Belgium, [¶]These authors contributed equally to this work.

ABSTRACT *In situ* click chemistry has been successfully applied to probe the ligand binding domain of EthR, a mycobacterial transcriptional regulator known to control the sensitivity of *Mycobacterium tuberculosis* to several antibiotics. Specific protein-templated ligands were generated *in situ* from one azide and six clusters of 10 acetylenic fragments. Comparative X-ray structures of EthR complexed with either clicked ligand BDM14950 or its azide precursor showed ligand-dependent conformational impacts on the protein architecture. This approach revealed two mobile phenylalanine residues that control the access to a previously hidden hydrophobic pocket that can be further exploited for the development of structurally diverse EthR inhibitors. This report shows that protein-directed *in situ* chemistry allows medicinal chemists to explore the conformational space of a ligand-binding pocket and is thus a valuable tool to guide drug design in the complex path of hit-to-lead processes.

Tuberculosis is a major cause of morbidity and mortality worldwide. This infectious disease caused by *Mycobacterium tuberculosis* kills each year between 1.2 and 1.8 million people (*1*). Although the combined use of four first-line antibiotics (izoniazid, rifampicin, pyrazinamide and ethambutol) known as directly observed treatment short-course (DOTS) claims to successfully treat 85% of the patients, multidrug-resistant strains of the mycobacteria rapidly emerge (*2*). Treatment of MDR-tuberculosis requires, for a longer period of time, the use of second line antibiotics that are less tolerated mainly due to lower therapeutic indexes, leading to noncompliance, relapse, and consequently increased mortality (*3*). While efforts are today focused on structure-based drug design and *in vitro* and *in vivo* screening to identify new drugs (*4, 5*) and evaluation of their combinations, our strategy relies on the improvement of existing therapies. Ethionamide, a second-line antibiotic, is one of the most widely used drugs for the treatment of multidrug-resistant tuberculosis; however, its use is hampered by severe side effects. Ethionamide itself is inactive and requires activation by the mycobacterial monooxygenase EthA to an active NAD-adduct that inhibits InhA, the enoyl-ACP reductase involved in mycolic acid biosynthesis (*6*–*8*). The expression of *ethA* is controlled by the transcriptional repressor EthR, a member of the TetR family of transcriptional regulators (*9, 10*). Genetic inactivation of *ethR* logically leads to overexpression of EthA and consequently to hypersensitivity of the mycobacteria to ethionamide (*6*).

We postulated that synthetic inhibitors of EthR would increase transcription of *ethA* and thus improve ethionamide bioactivation and efficacy. The first inhibitor of EthR, BDM14500, was identified through the screening of 131 compounds designed on the basis of the crystal structure of EthR. Hit-to-lead optimization was then performed *via* a rational design. We confirmed that all inhibitors occupy the ligand binding site of the protein, resulting in a global reorganization of its DNA binding domains, which leads to the inability of EthR to bind to its DNA operator. This procedure eventually led to the identification of compounds that significantly boost the antimycobacterial activity of ethionamide *in vitro* and *in vivo* in *M. tuberculosis*-infected mice, thus validating the ethionamide boosting concept (*11*).

During the hit-to-lead process, EthR binding of potent inhibitors was monitored by X-ray crystallography. Surprisingly one compound (BDM31381) adopted a new orientation compared to the initial hit by pointing its thienoacetyl substituent to the bottom of the pocket (*10*). This observation stimulated us to design new analogues to

*Corresponding authors, nicolas.willand@univ-lille2.fr, benoit.deprez@univ-lille2.fr.

Received for review March 18, 2010 and accepted August 12, 2010.

Published online August 12, 2010

10.1021/cb100177g

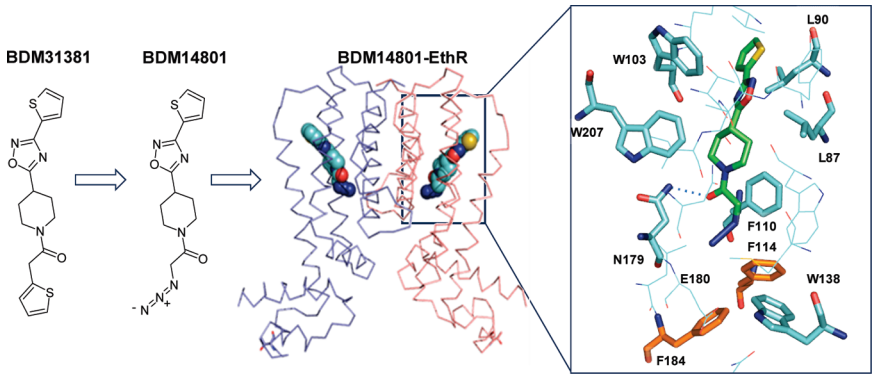

Figure 1. X-ray structure of azido ligand BDM14801 co-crystallized with mycobacterial transcriptional repressor EthR. Colors legend: green (ligand) and light blue (EthR) = carbon, dark blue = nitrogen, red = oxygen, dotted lines = hydrogen bonds. Key flexible residues are highlighted in yellow. The representations were generated from density maps using PyMol.

explore the ligand binding pocket of the protein and experimentally probe its ability to adopt new conformations upon binding of more extended ligands. An interesting question was whether yet unobserved conformations of the protein could be recruited *in situ* by diverse reagents in a click chemistry experiment. An extended binding pocket would provide an opportunity for the design of structurally diverse if not larger ligands. In the past 10 years, approaches based on the use of proteins as catalysts to covalently assemble fragments have been more and more successful. The concept of kinetic target-guided synthesis (TGS) (*12–14*) is based on the use of protein pockets to catalyze an irreversible reaction between two sets of complementary reactants. In particular, *in situ* click chemistry has emerged as the reaction of choice to produce efficiently potent triazole inhibitors of enzymes (acetylcholine esterase, carbonic anhydrase, or HIV protease) (*15–21*). So far, kinetic TGS approaches have been applied to the development of protein inhibitors and more recently to the discovery of protein−protein interaction modulators (*22*). The Huisgen 1,3-dipolar cycloaddition between azides and alkynes that yields triazoles was chosen for EthR-catalyzed synthesis. This reaction has the advantage of being performed in biocompatible solutions and in addition does not require external reagents or metal catalysts that might denature the protein. The first step was to identify an analogue of BDM31381 that could serve as template for this reaction. Among the compounds tested, the replacement of the thienoacetyl group in BDM31381 by an acetylazido group led to the discovery of BDM14801. This compound proved to retain affinity for the protein by inhibiting EthR-DNA interaction with an IC_{50} of 7.4 μM. Moreover co-crystallization of EthR with BDM14801 and X-ray diffraction showed the compound embedded in a similar orientation as BDM31381 in the ligand binding domain. The oxadiazole ring of the ligand is involved in a T-shape interaction with Trp103 while the amide function is H-bonded to Asn179. Importantly the azido function points to the hydrophobic bottom of the pocket closed by Phe114, Phe184, and Trp138 (Figure 1). BDM14801 was therefore the candidate of choice to start *in situ* click chemistry experiments designed to explore flexibility and accessibility of the bottom of the ligand binding pocket of EthR.

Sixty different aromatic or aliphatic alkynes were selected for their potential ability to interact with the hydrophobic portion of the ligand-binding pocket close to the azido function of BDM14801 (Figure 2, panel a). The selected alkynes were rationally distributed into six clusters of 10, in such a way that in case of condensation between multiple couples of reagents the resulting mixture of products would display different molecular weights (Supplementary Tables 1 and 2). Each cluster (containing 10 individual alkynes at 40 μM each) was incubated with BDM14801 (125 μM) and EthR (5 μM) for 5 days at 37 °C. Concentration of reagents was defined to ensure that at least a 1:1 ratio of synthesized triazole and protein would be obtained. In parallel, the same mixtures were prepared and incubated in the absence of EthR or with bovine serum albumin (BSA) to evaluate possible non EthR-specific protein-based catalysis. Analysis of the 18 reaction mixtures by SIM-LC/MS confirmed that the predominant product formed upon EthR-templated conditions is 4-iodobenzenesulfonamide triazole derivative (Figure 2, panel b). Comparison of LC/MS traces of protein-templated product with the corresponding 1,5- and 1,4-regioisomers, synthesized under thermal or copper iodide catalytic conditions, respectively, revealed that 1,4-regioisomer, referred to as BDM14950, is the main kinetic product of the reaction (Figure 2, panel c). Analysis of X-ray structures of EthR co-crystallized with BDM14801 and with BDM14950 revealed that both compounds occupy the two ligand-binding pockets of the homodimeric repressor. More importantly, atoms that BDM14801 and BDM14950 have in common occupy equivalent positions in the ligand-binding pocket (Figure 3). More precisely, the 4-(3-thiophen-2-yl-[1,2,4]oxadiazol-5-yl)-piperidine motif of each compound faces Leu87, Leu90, Trp103, and Trp207. The amide group of the side chain of Asn179 is hydrogen-bonded to the oxygen of the amide linker of the ligands (Figure 4, panels a and b). However, in contrast to the binding of BDM14801 to EthR, the binding of BDM14950 leads to structural modifica-

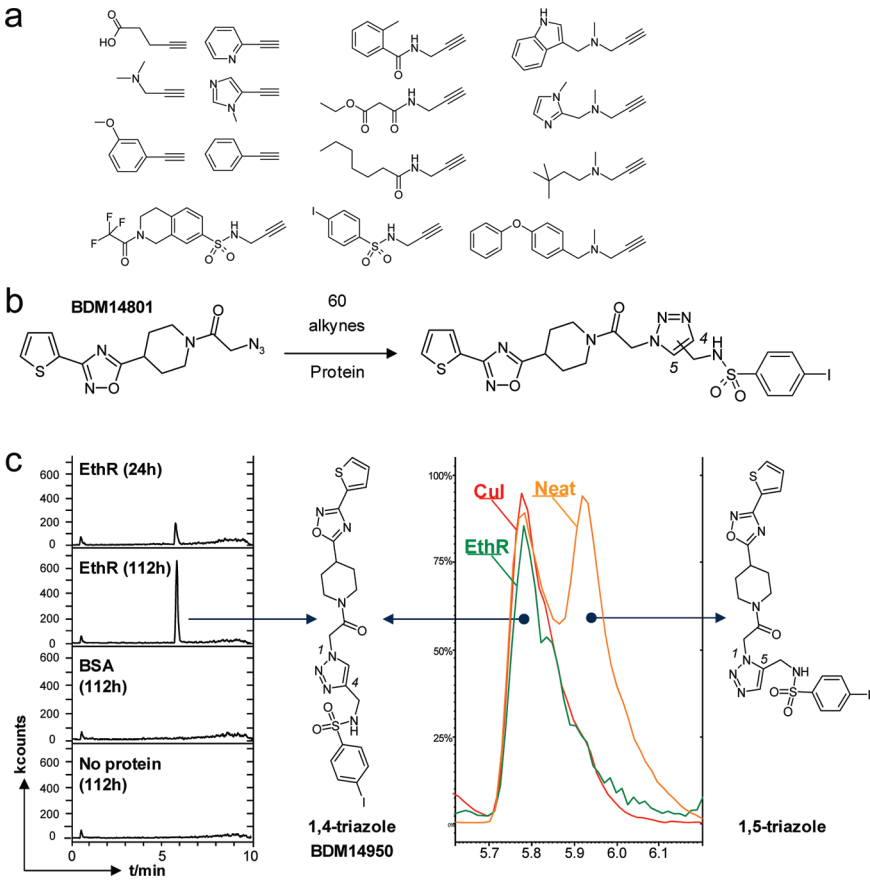

Figure 2. *In situ* click chemistry synthesis and analysis. a) Representative set of 15 alkynes. b) Scheme of *in situ* click chemistry synthesis. c) Single ion monitoring LC/MS (SIM-LC/MS) confirmation of *in situ* synthesis of 1,4-triazole BDM14950 regioisomer.

tions of the deeper portion of the pocket to accommodate the bulkier arylsulfonamide motif. In particular, BDM14950 induces displacement of Phe184 and Phe114, which tilt their side chain in order to allow the arylsulfonamide motif to gain access to a hydrophobic "back pocket" of the protein. The phenyl ring thus establishes strong van der Waals contacts with Trp138, while Gln125 is displaced and Arg128 is recruited through the formation of a network of hydrogen bonds involving Glu180 (Figure 4, panel b).

Both arginine and glutamine are known to be more flexible than most other residues except lysine. In contrast, phenylalanine shows the lowest propensity for flexibility (*23*). Here, the *in situ* assembly of BDM14950 within the ligand-binding domain of EthR was made possible only by the recruitment of a different conformation of the receptor. Indeed two phenylalanines have moved significantly their side chain to yield an "open-gate" conformation. In order to correlate these structural differences between the two complexes, with functional activity, BDM14950 was compared with the original azide in our SPR assay designed to evaluate the capacity of compounds to inhibit the binding of the repressor to its DNA operator. BDM14950 displayed an activity 10-fold higher (IC_{50} = 580 nM) than that of the corresponding azide (IC_{50} = 7.4 μM) (Supplementary Figure 1). This data confirms that the conformational change induced by BDM14950 anchoring remains compatible with the reorganization of the helix−turn−helix motifs that prevent DNA binding.

In conclusion, whereas BDM14801/EthR complex was shown to adopt a "closed-gate" conformation (Figure 5, panel a), binding of BDM14950 to EthR forces the protein to adopt an "open-gate" conformation (Figure 5, panel b) revealing a deeper, yet hidden, hydrophobic tunnel that may now be exploited for the development of new EthR inhibitor chemotypes.

Protein flexibility is a real challenge for the medicinal chemist. It makes the understanding of structure−activity relationships difficult and the rational design of compounds even more difficult, reducing in practice the strategy to a trial and error gameplay. However, flexibility of a binding domain can also represent an opportunity to explore a larger diversity of ligands. This has been recently exemplified by Garcin *et al.*, who have been able to optimize the selectivity of a series of NOS inhibitors by exploiting the difference in plasticity of the binding sites of the two closely related isoforms iNOS and eNOS (*24*). Therefore all reliable means to detect, assess, or model the flexibility of a ligand binding pocket are highly desirable in the context of drug discovery. Handling receptor flexibility *in silico* remains today a challenge and the simulation of the relevant protein conformations for a given ligand can only be achieved with a combination of methods (*25*). *In silico* docking based on X-ray diffraction data is frequently considered to assist drug discovery during hit-to-lead and lead optimization. This approach is, however, often limited by the inherent rigid model issued from crystallography. As proteins are not structurally static but adopt spontaneously a variety of conformations (*26*), new molecular docking methods have been introduced to take into account both ligand and receptor flexibility

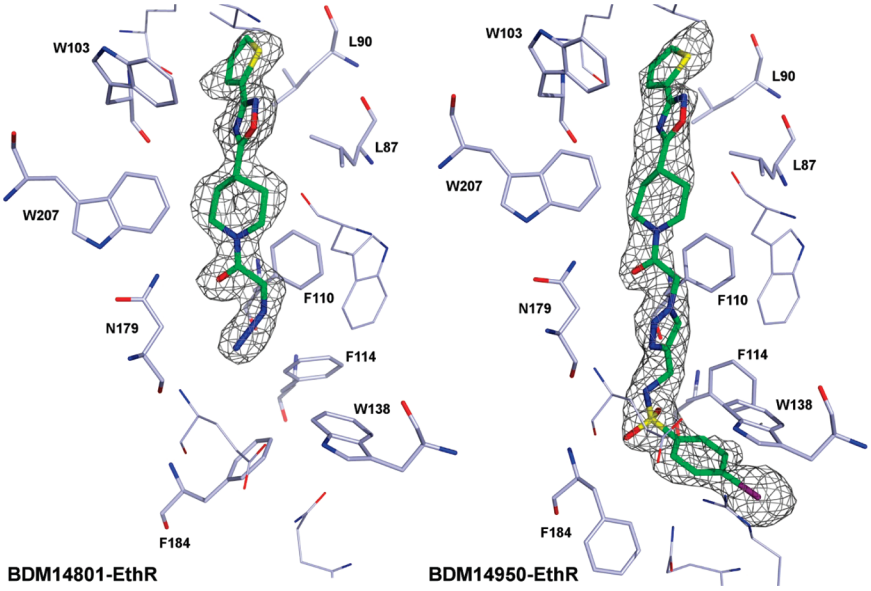

Figure 3. X-ray structure representations of the ligand-binding pocket of EthR filled with BDM14801 and BDM14950 surrounded by their respective initial F_o-F_c map at 3.0 σ contour level. F_o-F_c maps were calculated prior to adding the ligand to the model. Colors legend: green (ligand) and light blue (EthR) = carbon, blue = nitrogen, red = oxygen, yellow = sulfur, purple = iodine.

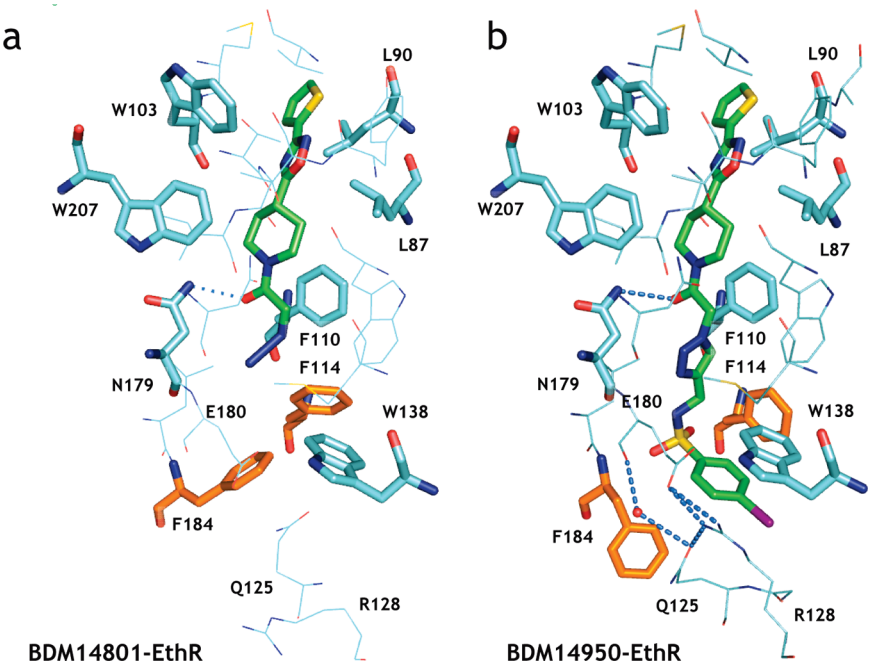

Figure 4. X-ray structure representations of the ligand-binding pocket of EthR. a) EthR filled with BDM14801. b) EthR filled with BDM14950. Colors legend: green (ligand) and light blue (EthR) = carbon, blue = nitrogen, red = oxygen, dotted lines = hydrogen bonds. Key flexible residues are highlighted in yellow. The representations were generated from density maps using PyMol.

(*27*). However, these methods require protracted computational time that can only be reduced by imposing limitations on the conformational space.

As the exploration of the upper part of the ligand binding domain of EthR with rationally designed inhibitors revealed that the conformation of amino acids surrounding the accessible pocket were weakly influenced by the structure of the ligands (*10*), we designed an *in situ* click chemistry approach to explore in detail the binding cavity in order to discover new accessible pockets. Ligands of EthR were generated according to a Huisgen 1,3-dipolar cycloaddition. The binding modes of the starting azide and the *in situ* generated triazole were compared using X-ray crystallography. This revealed the dual nature of the ligand-binding pocket of the protein: the upper part of the binding pocket is structurally conserved, whereas the bottom part undergoes important rearrangement. Hit compound BDM14500 and optimized analogue BDM31381 revealed only the less flexible subdomain of the ligand binding pocket. Consequently, classical docking experiments would have been efficient only for the exploration of this subregion. In contrast, the protein-directed in situ synthesis used here revealed a previously hidden binding pocket of EthR that can now be explored to develop a new series of ligands with original binding modes. Although the protein-templated *in situ* click chemistry approach developed in this study did not deliver improved EthR inhibitors, it has led to a much better understanding of the target and provides additional evidence that the combination of crystallography and *in situ* click chemistry is highly valuable in the field of drug discovery.

With this report, we show that *in situ* click chemistry not only is dedicated for the discovery of optimized inhibitors of enzymes but also allows one to explore the conformational space of flexible ligand binding domain, including the one of tran-

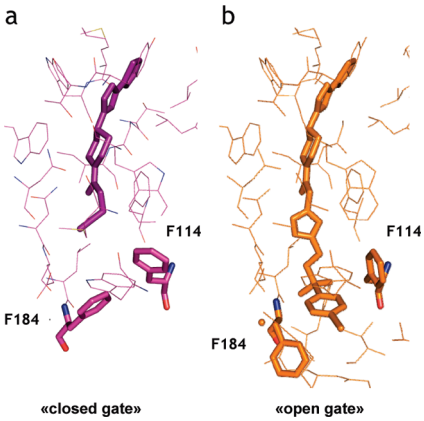

Figure 5. X-ray structure representations of the ligand-binding pocket of EthR showing the mobility of Phe114 and Phe184. a) EthR filled with BDM14801. b) EthR filled with BDM14950. Colors legend: blue = nitrogen, red = oxygen, hatched lines = hydrogen bonds. Essential residues of the protein are highlighted with sticks. The representations were generated from density maps using PyMol.

scriptional repressors. More importantly all the binding pocket conformations observed can now be used to design structurally diverse ligands that are expected to all remain inhibitors. We thus believe that it is a valuable tool to guide drug design in the complex path of the hit-to-lead process. In particular what has been achieved here with a bacterial ligand-dependent transcription factor could certainly be applied to human nuclear hormone receptors (NHRs), which are known to often display a high degree of flexibility that poses difficulties for rational drug design.

METHODS

General. All reagents and solvents were purchased from commercial sources and used without further purification. Reactions were performed under air and monitored by TLC and LCMS when possible. Flash chromatography was performed on AIT system. Mass spectra were recorded on a LC-MS-MS triple-quadrupole system (Varian 1200ws). HPLC analysis was performed using a C^{18} TSK-GEL Super ODS column, dimensions 4.6 mm × 50 mm. LCMS gradient starting from 100% H_2O/0.1% formic acid and reaching 20% H_2O/80% CH_3CN/0.08% formic acid within 10 min at a flow rate of 1 mL min^{-1} was used. ^1H and ^{13}C NMR spectra were recorded on a Bruker 300 MHz spectrometer. Chemical shifts in ^1H NMR are reported in parts per million (ppm) on the δ scale from an internal standard of residual deuterated chloroform, dimethylformamide, dichloromethane, or DMSO. Data from ^{13}C spectra were reported in terms of chemical shift in ppm from the center peak of $CDCl_3$, CD_2Cl_2, DMF-d_7 or DMSO-d_6. Melting points were determined on a Büchi B-540 apparatus and are uncorrected.

***In Situ* Click Chemistry Protocol.** Each of the 60 alkynes was solubilized in 250 μL of methanol to reach a final concentration of 80 mM. The six clusters of 10 alkynes were constituted by mixing 35 μL of the 10 required alkyne solutions to reach a final concentration of 8 mM per compound in 350 μL of methanol. For each cluster, 4 deep wells of the corresponding line of the plate were filled with 3 μL of the respective acetylenic mixture, 3 μL of azide at 25 mM in methanol: deep wells of row 1 were filled with 600 μL of EthR at 5 μM solubilized in Tris buffer (Tris 10 mM, pH = 7.5, NaCl 200 mM, EDTA 0.1 mM, DTT 1 mM), deep wells of row 2 were filled with 600 μL of Tris buffer, deep wells of row 3 were filled with BSA at 5 μM solubilized in Tris buffer, and deep wells of row 4 were filled with 600 μL of CuI at 4 mM in acetonitrile. Each reaction mixture was incubated at 37 °C for 96 h. Samples of the reactions (100 μL) were diluted in MeOH (100 μL) and injected (10 μL) for LC-MS-SIM analysis.

LC-MS/MS Analysis. The LC-MS/MS system consisted of a Varian 1200 L, a Prostar 430 autosampler, a triple quadrupole mass spectrometry equipped with an electrospray ionization source, with a Prostar 325 detector. Analytes in incubation mixtures were separated by HPLC using a gel TSK C18 Super-ODS, 5 μm, 50 mm × 4.6 mm column. LCMS gradient starting from 100% H_2O/0.1% formic acid and reaching 20% H_2O/80% CH_3CN/0.08% formic acid within 10 min at a flow rate of 1 mL min^{-1} was used. The injection volume was 10 μL; 30% of the eluent was introduced into the triple quadrupole mass spectrometer source. The source temperature of the mass spectrometer was maintained at 300 °C, the declustering potential was 50 V, and the curtain gas pressure is 1.5 mTorr.

Chemical Synthesis of 2-Azido-1-[4-(3-thiophen-2-yl-[1,2,4]oxadiazol-5-yl)-piperidin-1-yl]-ethanone (BDM14801). In a round-bottom flask (250 mL) was introduced 4-(3-thiophen-2-yl-[1,2,4]oxadiazol-5-yl)-piperidine-1-carboxylic acid *tert*-butyl ester (1.1 g, 3.28 mmol, 1 equiv), and 7 mL of ethanol was added. 4 N HCl in dioxane (1 mL, 4 mmol, 1.05 mmol) was added to the solution. The mixture was heated at 50 °C for 2 h. The reaction was cooled down, and 10 mL of diethyl ether was added. The precipitate was filtered to give 9.56 g of a beige powder. ^1H NMR (DMSO-d_6): 2.00 (qd, J = 11.5 Hz, J = 3.0 Hz, 2H); 2.25 (dd, J = 11.5 Hz, J = 3.0 Hz, 2H), 3.10 (q, J = 10.2 Hz, 2H), 3.30 (d, J = 11 HZ, 2H), 3.50 (m, 1H), 7.26 (dd, J = 5.0 Hz, 3.70 Hz), 7.78 (dd, J = 3.5 Hz, J = 1.1 Hz), 7.85 (dd, J = 5.0 Hz, J = 1.2 Hz). LCMS m/z: 236 $[M + H]^+$. 4-(3-Thiophen-2-yl-[1,2,4]oxadiazol-5-yl)-piperidinium hydrochloride (168 mg, 0.6 mmol, 1 equiv) and triethylamine (220 μL, 1.9 mmol, 3.1 equiv) were mixed in dichloromethane (1 mL) and cooled to −15 °C. Chloroacetyl chloride (40 μL, 0.6 mmol, 1 equiv) was added dropwise over 10 min. The resulting mixture was stirred at RT for 2 h. Dichloromethane (20 mL) was added to the solution, and the organic layer was washed 3 times with 15 mL of hydrochloric acid solution (5%) and then with 15 mL of brine and dried over $MgSO_4$. The organic layer was reduced under pressure to give 2-chloro-1-[4-(3-thiophen-2-yl-[1,2,4]oxadiazol-5-yl)-piperidin-1-yl]-ethanone as a white solid with 95% yield. ^1H NMR ($CDCl_3$): 2.00 (m, 2H); 2.19 (m, 2H); 3.08 (m, 1H); 3.29 (m, 2H); 3.95 (m, 1H); 4.12 (s, 2H, CH_2); 4.45 (m, 1H); 7.17 (dd, J = 5.0 Hz, J = 3.0 Hz, 1H); 7.53 (d, J = 5.0 Hz, 1H); 7.80 (d, J = 3.0 Hz, 1H). LCMS m/z: 312 $[M + H]^+$. 2-Chloro-1-[4-(3-thiophen-2-yl-[1,2,4]oxadiazol-5-yl)-piperidin-1-yl]-ethanone (312 mg, 1 mmol, 1 equiv) was dissolved in 1 mL of DMF. Sodium azide (91 mg, 1.4 mmol, 1.4 equiv) was added to the solution, and the mixture was stirred at RT for 18 h. The solution was reduced under pressure, and the residue was dissolved in 50 mL of ethylacetate. The organic layer was washed with 20 mL of $KHSO_4$ solution (0.1 N), 20 mL of saturated $NaHCO_3$ solution, and 2 times with 20 mL of brine. The organic layer was dried over $MgSO_4$, filtered, and reduced under pressure to give 2-azido-1-[4-(3-thiophen-2-yl-[1,2,4]oxadiazol-5-yl)-piperidin-1-yl]-ethanone as a beige solid with a 80% yield. ^1H NMR ($CDCl_3$): 1.95 (m, 2H); 2.20 (m, 2H); 3.06 (m, 1H); 3.27 (m, 2H); 3.74 (d, 1H, J = 13.5 Hz); 3.99 (s, 2H); 4.45 (d, 1H, J = 13.5 Hz); 7.14 (dd, J = 5.0 Hz, J = 3.0 Hz, 1H); 7.50 (d, J = 5.0 Hz, 1H); 7.78 (d, J = 3.0 Hz, 1H). ^{13}C NMR ($CDCl_3$): 28.7; 29.4; 34.0; 41.2; 44.2; 50.9; 128.1; 129.4; 129.6; 164.4; 165.5; 180.4; LCMS m/z: 319 $[M + H]^+$.

Chemical Synthesis of 4-Iodo-*N*-(1-{2-oxo-2-[4-(3-thiophen-2-yl-1,2,4-oxadiazol-5-yl)-piperidin-1-yl]-ethyl}-1*H*-1,2,3-triazol-4-ylmethyl)-benzenesulfonamide (BDM14950). In a Wheaton tube (1 mL) were introduced 2-azido-1-[4-(3-thiophen-2-yl-[1,2,4]oxadiazol-5-yl)-piperidin-1-yl]-ethanone BDM14801 (19 mg, 59 μmol, 1 equiv) and 4-iodo-*N*-prop-2-ynyl-benzenesulfonamide (**3**) (59 μmol, 1 equiv) in 200 μL of CH_3CN. Copper iodide (2 mg) was added under stirring. The solution was stirred at RT for a further 18 h. The organic layer was filtered and washed with cold CH_3CN to give the desired compound as a beige powder. Yield: 69%. ^1H NMR (DMF-d_7): 1.76 (m, 1H); 2.04 (m, 1H); 2.21 (m, 2H); 3.00 (m, 1H); 3.48 (m, 1H); 3.51 (m, 1H); 4.14 (m, 1H); 4.24 (s, 2H); 4.42 (m, 1H); 5.60 (m, 2H); 7.33 (m, 1H); 7.70 (m, 2H); 7.87 (m, 1H); 7.94 (m, 2H); 8.09 (m, 2H); 8.20 (brs, 1H). ^{13}C NMR (DMF-d_7): 30.0; 30.1; 33.8; 38.7; 41.0; 43.8; 50.9; 99.6; 125.1; 128.1; 128.5; 128.6; 129.9; 130.4; 138.4; 140.8; 143.5; 164.1; 164.4; 182.0. LCMS (EI(+)) m/z: 640 $[M + H]^+$.

SPR Assay. SPR analysis of the molecular interactions between EthR and the *ethA* promoter region was performed using research grade CM5 sensor chips on a BIAcore2000 instrument. Streptavidin was injected onto the CM5 sensor

chips at 500 ng mL^{-1} in 10 mM sodium acetate (pH 3.5) for 12 min at a flow rate of 10 $\mu L\ min^{-1}$. The 106-bp biotinylated DNA fragment overlapping the *ethA-ethR* intergenic region was obtained by polymerase chain reaction (PCR), purified by agarose gel electrophoresis, and immobilized onto the CM5 sensor chip. The biotinylated DNA fragment was injected in one channel of the chip at 200 ng mL^{-1} to obtain a 50 resonance unit (RU) stable fixation to streptavidin. Another channel of the chip was loaded with a biotinylated double stranded 113-bp long irrelevant DNA fragment (+14 to +127 fragment of the *E. coli* bla gene PCR amplified using oligonucleotides O-343: TTTCCGTGTCGCCCTTATTCC and O-344: CCACTCGTGCACCCAACTGAT and pUC18 as substrate). Binding of EthR to the immobilized DNA was performed at 25 °C in 10 mM Tris-HCl (pH 7.5), 200 mM NaCl, 0.1 mM EDTA, 1 mM DTT, and 1% DMSO at a flow rate of 20 $\mu L\ min^{-1}$. Specific interaction (SI) between EthR and the 106-bp DNA fragment was defined as the signal difference between both channels. For dose response curves establishment, the test compounds were serially diluted in the binding buffer containing 540 nM EthR, incubated 5 min at 37 °C, and then injected in the BIAcore at a flow rate of 20 $\mu L\ min^{-1}$ for 3 min. SI values were measured at the end of the injection period and used to calculate the inhibition of protein−DNA interaction. IC_{50} values were determined by using the XLFit software.

Crystal Structure Determination of EthR−Ligand Complexes. N-Terminally hexa-histidine-tagged EthR was produced in *E. coli* C41 (pET-15b- ethR) and purified as previously described (*8*). Prior to crystallization, the protein was buffer exchanged against 10 mM Tris-HCl (pH 7.5), 200 mM NaCl and concentrated to 26 mg mL^{-1}. Crystals were obtained by the vapor diffusion method, using 0.1 mM Mes pH 6.5, 1.5 M ammonium sulfate, and 20% glycerol as the crystallization solution. Ligands were dissolved in 100% DMSO. Prior to crystallization, the protein was incubated with the ligand, either BDM14801 or BDM14950, added at equimolar concentration. The crystals belong to space group $P4_12_12$. Data collection statistics are summarized in Supplementary Table 3. The diffraction data were processed with XDS (*28*). The structures have been determined by molecular replacement using as the initial coordinates the EthR structure deposited in the protein data bank (PDB code 1U9N). The structures were refined using REFMAC5 (*29*) from the CCP4 suite (*30*) to a resolution of 1.9 Å. The ligands were positioned in the electron density with COOT (*31*). The final Rwork (Rfree) (*32*) for BDM14801 and BDM14950 are 18.2% (22.1%) and 19.3% (25.1%), respectively.

Accession Codes: Structure factors and final coordinates have been deposited in the RCSB PDB with ID codes 3O8G and 3O8H for BDM14801 and BDM14950, respectively.

Acknowledgment: This work was supported by INSERM, University of Lille 2, Institut Pasteur de Lille, CNRS, Région Nord-Pas de Calais, EU, FEDER (OBJ2-4.1-2006/3-n°297/9360), and ANR (ANR-06-EMPB-033). We are indebted to the ESRF (Group BAG MX-485). B.D. is a recipient of a doctoral fellowship MENR. Z.L. is a fellow of the F.R.S.-FNRS. We thank Prof. André Tartar and Dr. Bruno Villoutreix for helpful discussions. We thank VARIAN Inc. for their technical support. RMN acquisitions were done by the LARMN, Lille.

Supporting Information Available: This material is available free of charge *via* the Internet at http://pubs.acs.org.

REFERENCES

1. World Health Organization (2009) *Global Tuberculosis Control: Epidemiology, Strategy, Financing*, pp 6−33, WHO, Geneva.
2. Cox, H. S., Ford, N., and Reeder, J. C. (2009) Are we really that good at treating tuberculosis? *Lancet Infect. Dis. 9*, 138−139.
3. Cox, H., Kebede, Y., Allamuratova, S., Ismailov, G., Davletmuratova, Z., Byrnes, G., Stone, C., Niemann, S., Rüsch-Gerdes, S., Blok, L., and Doshetov, D. (2006) Tuberculosis recurrence and mortality after successful treatment: impact of drug resistance, *PLoS Med. 3*, 1836−1843.
4. Zhang, Y., Post-Martens, K., and Denkin, S. (2006) New drug candidates and therapeutic targets for tuberculosis therapy, *Drug Discovery Today 11*, 21−27.
5. Terwilliger, T. C., *et al.* (2003) The TB structural genomics consortium: a resource for *Mycobacterium tuberculosis* biology, *Tuberculosis 83*, 223−249.
6. DeBarber, A. E., Mdluli, K., Bosman, M., Bekker, L. G., and Barry, C. E., 3rd (2000) Ethionamide activation and sensitivity in multidrug-resistant *Mycobacterium tuberculosis*, *Proc. Natl Acad. Sci. U.S.A. 97*, 9677−9682.
7. Baulard, A. R., Betts, J. C., Engohang-Ndong, J., Quan, S., McAdam, R. A., Brennan, P. J., Locht, C., and Besra, G. S. (2000) Activation of the pro-drug ethionamide is regulated in mycobacteria, *J. Biol. Chem. 275*, 28326−28331.
8. Wang, F., Langley, R., Gulten, G., Dover, L. G., Besra, G. S., Jacobs, W. R., Jr., and Sacchettini, J. C. (2007) Mechanism of thioamide drug action against tuberculosis and leprosy, *J. Exp. Med. 204*, 73−78.
9. Engohang-Ndong, J., Baillat, D., Aumercier, M., Bellefontaine, F., Besra, G. S., Locht, C., and Baulard, A. R. (2004) EthR, a repressor of the TetR/CamR family implicated in ethionamide resistance in mycobacteria, octamerizes cooperatively on its operator, *Mol. Microbiol. 51*, 175−188.
10. Ramos, J. L., Martinez-Bueno, M., Molina-Henares, A. J., Teran, W., Watanabe, K., Zhang, X., Gallegos, M. T., Brennan, R., and Tobes, R. (2005) The TetR family of transcriptional repressors, *Microbiol. Mol. Biol. Rev. 69*, 326−356.
11. Willand, N., Dirie, B., Carette, X., Bifani, P., Singhal, A., Desroses, M., Leroux, F., Willery, E., Mathys, V., Deprez-Poulain, R., Delcroix, G., Frenois, F., Aumercier, M., Locht, C., Villeret, V., Deprez, B., and Baulard, A. R. (2009) Synthetic EthR inhibitors boost antituberculous activity of ethionamide, *Nat. Med. 15*, 537−544.
12. Inglese, J., and Benkovic, S. J. (1991) Multisubstrate adduct inhibitors of glycinamide ribonucleotide transformylase: synthetic and enzyme-assembled, *Tetrahedron 47*, 2351−2364.
13. Régis, N., and Ivan, H. (2001) Using an enzyme's active site to template inhibitors, *Angew. Chem., Int. Ed. 40*, 1774−1776.
14. Sharpless, K. B., and Manetsch, R. (2006) In situ click chemistry: a powerful means for lead discovery, *Exp. Opin. Drug Discovery 1*, 525−538.
15. Mamidyala, S. K., and Finn, M. G. (2010) In situ click chemistry: probing the binding landscapes of biological molecules, *Chem. Soc. Rev. 39*, 1252−1261.
16. Warren, G. L., Luke, G. G., Flavio, G., Zoran, R., cacute, Paul, R. C., Palmer, T., Finn, M. G., and Sharpless, K. B. (2002) Click chemistry in situ: acetylcholinesterase as a reaction vessel for the selective assembly of a femtomolar inhibitor from an array of building blocks, *Angew. Chem., Int. Ed. 41*, 1053−1057.
17. Manetsch, R., Krasinski, A., Radic, Z., Raushel, J., Taylor, P., Sharpless, K. B., and Kolb, H. C. (2004) In situ click chemistry: enzyme inhibitors made to their own specifications, *J. Am. Chem. Soc. 126*, 12809−12818.
18. Krasinski, A., Radic, Z., Manetsch, R., Raushel, J., Taylor, P., Sharpless, K. B., and Kolb, H. C. (2005) In situ selection of lead compounds by click chemistry: target-guided optimization of acetylcholinesterase inhibitors, *J. Am. Chem. Soc. 127*, 6686−6692.
19. Mocharla, V. P., Colasson, B., Lee, L. V., Roper, S., Sharpless, K. B., Wong, C. H., and Kolb, H. C. (2004) In situ click chemistry: enzyme-generated inhibitors of carbonic anhydrase II, *Angew. Chem., Int. Ed. 44*, 116−120.
20. Jinyi, W., Guodong, S., Vani, P. M., Rachel, J. L., Michael, E. P., Hartmuth, C. K., and Hsian-Rong, T. (2006) Integrated microfluidics for parallel screening of an in situ click chemistry library, *Angew. Chem., Int. Ed. 45*, 5276−5281.
21. Whiting, M., Muldoon, J., Lin, Y. C., Silverman, S. M., Lindstrom, W., Olson, A. J., Kolb, H. C., Finn, M. G., Sharpless, K. B., Elder, J. H., and Fokin, V. V. (2006) Inhibitors of HIV-1 protease by using in situ click chemistry, *Angew. Chem., Int. Ed. 45*, 1435−1439.
22. Hu, X., Sun, J., Wang, H.-G., and Manetsch, R. (2008) Bcl-XL-templated assembly of its own protein-protein interaction modulator from fragments decorated with thio acids and sulfonyl azides, *J. Am. Chem. Soc. 130*, 13820−13821.
23. Najmanovich, R., Josef, K., Sobolev, V., and Edelman, M. (2000) Side-chain flexibility in proteins upon ligand binding, *Proteins: Struct., Funct., Genet. 39*, 261−268.
24. Garcin, E. D., Arvai, A. S., Rosenfeld, R. J., Kroeger, M. D., Crane, B. R., Andersson, G., Andrews, G., Hamley, P. J., Mallinder, P. R., Nicholls, D. J., St-Gallay, S. A., Tinker, A. C., Gensmantel, N. P., Mete, A., Cheshire, D. R., Connolly, S., Stuehr, D. J., Aberg, A., Wallace, A. V., Tainer, J. A., and Getzoff, E. D. (2008) Anchored plasticity opens doors for selective inhibitor design in nitric oxide synthase, *Nat. Chem. Biol. 4*, 700−707.
25. B-Rao, C., Subramanian, J., and Sharma, S. D. (2009) Managing protein flexibility in docking and its applications, *Drug Discovery Today 14*, 394−400.

26. Kenakin, T., and Onaran, O. (2002) The ligand paradox between affinity and efficacy: can you be there and not make a difference? *Trends Pharmacol. Sci. 23*, 275–280.
27. Wong, C. F. (2008) Flexible ligand-flexible protein docking in protein kinase systems, *Biochim. Biophys. Acta, Proteins Proteomics 1784*, 244–251.
28. Kabsch, W. (2010) XDS, *Acta Crystallographica Section D 66*, 125–132.
29. Winn, M. D., Isupov, M. N., and Murshudov, G. N. (2001) Use of TLS parameters to model anisotropic displacements in macromolecular refinement, *Acta Crystallogr., Sect. D: Biol. Crystallogr. 57*, 122–133.
30. Collaborative-Computational-Project-Number-4. (1994) The CCP4 suite: programs for protein crystallography, *Acta Crystallogr., Sect. D: Biol. Crystallogr. 50*, 760–763.
31. Emsley, P., and Cowtan, K. (2004) Coot: model-building tools for molecular graphics, *Acta Crystallogr., Sect. D: Biol. Crystallogr. 60*, 2126–2132.
32. Brunger, A. T. (1992) Free R value: a novel statistical quantity for assessing the accuracy of crystal structures, *Nature 355*, 472–474.